VARIATIONAL MONTE CARLO CALCULATIONS FOR BOSE-HUBBARD MODEL BASED ON PROJECTED WAVEFUNCTIONS

A THESIS

SUBMITTED TO THE DEPARTMENT OF PHYSICS

AND THE GRADUATE SCHOOL OF ENGINEERING AND SCIENCE

OF BILKENT UNIVERSITY

IN PARTIAL FULFILLMENT OF THE REQUIREMENTS

FOR THE DEGREE OF

MASTER OF SCIENCE

By

Fulya Koç

June, 2014

I certify that I have read this thesis and that in my opinion it is fully adequate, in scope and in quality, as a thesis for the degree of Master of Science.

Asst. Prof. Dr. Balazs Hetényi(Advisor)

I certify that I have read this thesis and that in my opinion it is fully adequate, in scope and in quality, as a thesis for the degree of Master of Science.

Prof. Dr. Cemal Yalabık

I certify that I have read this thesis and that in my opinion it is fully adequate, in scope and in quality, as a thesis for the degree of Master of Science.

Assoc. Prof. Dr. Azer Kerimov

Approved for the Graduate School of Engineering and Science:

Prof. Dr. Levent Onural
Director of the Graduate School

ABSTRACT

VARIATIONAL MONTE CARLO CALCULATIONS FOR BOSE-HUBBARD MODEL BASED ON PROJECTED WAVEFUNCTIONS

Fulya Koç
M.S. in Physics
Supervisor: Asst. Prof. Dr. Balazs Hetényi
June, 2014

Bose-Hubbard model is mainly used to describe and study the interactions between neutral atomic gases trapped in an optical lattice [1] and Josephson junction arrays [2]. It is one of the toy models to understand quantum phase transitions, i.e. a phase transition exists between the Mott insulator state and the superfluid state. Analytical solutions are limited to obtaining the ground state energy for small systems, whereas, computational studies can be done for larger system sizes. We applied the variational Monte Carlo method to the Bose-Hubbard model based on projected wavefunctions, i.e. Baeriswyl and Gutzwiller-Baeriswyl. Even though our method can be applicable to any dimension, we only consider the one dimensional case in this thesis. We expressed observables in forms of averages over configurations to which we can apply Monte Carlo sampling techniques. Our results for both Baeriswyl and Gutzwiller projections are in qualitatively good agreement with the known calculations of the phase diagram [3, 4]. Furthermore, we introduced a new method, apart from other known methods [5, 6], based on the Drude weight [7–9] to calculate the superfluid fraction, which can also be extended to observe BCS superconductivity [10].

Keywords: Bose-Hubbard model, Gutzwiller, Baeriswyl, Variational Monte Carlo.

ÖZET

BOSE-HUBBARD MODELİ İÇİN İZDÜŞÜMLÜ DALGA FONKSİYONLARI KULLANARAK VARYASYONEL MONTE CARLO HESAPLAMALARI

Fulya Koç
Fizik, Yüksek Lisans
Tez Yöneticisi: Asst. Prof. Dr. Balazs Hetényi
Haziran, 2014

Bose-Hubbard modeli, genel anlamda, optik kafes içerisine sıkışmış nötr gazlar arasındaki etkileşimler [1] ile Josephson eklemlerini [2] incelemek için kullanılır. Bose-Hubbard Hamiltonian'ı, kuvantum faz geçişlerini, Mott yalıtkanı fazı ile süperakışkan fazı arası geçişi, anlamak için en temel modeli oluşturur. Analitik çözümler küçük sistemlerle sınırlı kalırken hesaplamalı çözümler daha büyük sistemleri anlamak için kullanılır. Bu tezde Bose-Hubbard modeli izdüşümsel dalga fonksiyonları, Baeriswyl ve Gutzwiller-Baeriswyl, kullanarak varyasyonel Monte Carlo yaklaşımı ile incelenmiştir. Geliştirdiğimiz metod herhangi bir boyuta uygulanabilmesine rağmen, bu tezde, sadece 1 boyutta hesaplamalar yapılmıştır. Fiziksel nicelikler Monte Carlo tekniklerini uygulayabileceğimiz şekilde konfigürasyonlar üzerinden ortalama hesapları yapılarak incelenmiştir. Elde ettiğimiz sonuçlar, daha önceki bulgularla [3,4] nitelik bakımından iyi şekilde örtüşmektedir. Ayrıca süperakışkan fazı oranını hesaplamak için daha önce kullanılan metodlardan [5, 6] daha farklı bir metod, Drude ağırlığı [7–9], için temel oluşturduk. Aynı zamanda bu metod BCS süperiletkenliğini açıklamak için de genişletilebilir [10].

Anahtar sözcükler: Bose-Hubbard modeli, Gutzwiller, Baeriswyl, Varyasyonel Monte Carlo.

Contents

List of Figures

Chapter 1

Introduction

1.1 Bose-Hubbard Model

The Bose-Hubbard model is a bosonic analogue of the Fermi-Hubbard model [11] which studies the strongly correlated materials. The Bose-Hubbard model was first introduced by Gersch and Knollman in 1963 [12], and further studied extensively by Fisher et al. in 1989 [13]. Based on the analysis of Fisher et al., the phase diagram of the Bose-Hubbard model at zero temperature contains two different phases, namely; *Mott insulating phase* and *superfluid phase*. Hamiltonian of the model is

$$\hat{H} = -t \sum_{<i,j>} \left(\hat{b}_i^\dagger \hat{b}_j + h.c. \right) + \frac{U}{2} \sum_i \hat{n}_i \left(\hat{n}_i - 1 \right) - \mu \sum_i \hat{n}_i \tag{1.1}$$

where $\hat{b}_i^\dagger$ and $\hat{b}_i$ boson creation and annihilation operators on site-i respectively. $\hat{n}_i = \hat{b}_i^\dagger \hat{b}_i$ is boson occupation number at site-i, and t is the hopping parameter. $< i, j >$ indicates that the summation over nearest neighboring sites. U, denotes on-site interaction; it can be either repulsive, $U > 0$, or attractive, $U < 0$. Finally, μ is the chemical potential.

Boson creation and annihilation operators obey the following commutation relations;

$$\left[\hat{b}_i, \hat{b}_j^\dagger\right] = \delta_{ij} \quad and \quad \left[\hat{b}_i^\dagger, \hat{b}_i^\dagger\right] = \left[\hat{b}_i, \hat{b}_i\right] = 0 \qquad \forall i, j \tag{1.2}$$

These operators also act on the eigenbasis of the single-site boson occupation number operator as;

$$\begin{aligned} \hat{b}_i^\dagger|\hat{n}_i> &= \sqrt{n_i+1}|n_i+1> \\ \hat{b}_i|\hat{n}_i> &= \sqrt{n_i}|n_i-1> \end{aligned} \tag{1.3}$$

The first term in (1.1) denotes the *hopping term* and it introduces hoppings of bosons between nearest neighboring sites. This term of the Hamiltonian, in a way, describes how particles are delocalized; hence, it is convenient to represent it as the kinetic term as well. Second term in (1.1), on the other hand, is called *on-site repulsion term*, which contrarily to the first term tries to localize the bosons on each site. The last term in (1.1) controls the particle number in the system.

In order to analyse the quantum phase transition and the existence of two phases as indicated at the beginning of this chapter, we need to consider two cases; first one is $\frac{t}{U} \to 0$ which corresponds to the localized case, i.e. Mott insulating phase, and the second one is $\frac{t}{U} \to \infty$ which corresponds to a delocalized case, i.e. superfluid phase. However before analysing these two limits, one needs to define the symmetries of the Bose-Hubbard Hamiltonian.

1.2 Symmetries of The Bose-Hubbard Hamiltonian

Basically, we can analyse the symmetry consideration of the Bose-Hubbard model in three different ways [14–16];

1. $U(1)$ Symmetry:

   This symmetry indicates the conservation of total number of particles in the system, and $\hat{H}$ is invariant under transformation;

$$\left(\hat{b}_i^\dagger, \hat{b}_i\right) \rightarrow \left(\hat{b}_i^\dagger e^{i\theta}, \hat{b}_i e^{-i\theta}\right) = e^{i\hat{N}\theta}\left(\hat{b}_i^\dagger, \hat{b}_i\right) e^{-i\hat{N}\theta} \qquad \forall\theta \in \Re \tag{1.4}$$

2. Translational Symmetry:

   This symmetry indicates the conservation of total quasi-momentum of particles in the system, and $\hat{H}$ is invariant under transformation;

$$\left(\hat{b}_{i+1}^\dagger, \hat{b}_{i+1}\right) \rightarrow e^{-i\hat{T}}\left(\hat{b}_i^\dagger, \hat{b}_i\right) e^{i\hat{T}} \tag{1.5}$$

   with $\hat{T}$ being;

$$\hat{T} = \sum_{k=0}^{L-1} \frac{2\pi k}{L} \hat{b}_i^\dagger \hat{b}_i \tag{1.6}$$

   where L is the lattice site.

3. Reflection Symmetry:

   In this symmetry $\hat{H}$ is invariant under transformation;

$$\begin{aligned} \left(\hat{b}_i^\dagger, \hat{b}_i\right) &\rightarrow \left(\hat{b}_{N-i}^\dagger, \hat{b}_{N-i}\right) \quad in \quad real \quad space \quad or \\ \left(\hat{b}_k^\dagger, \hat{b}_k\right) &\rightarrow \left(\hat{b}_{-k}^\dagger, \hat{b}_{-k}\right) \quad in \quad momentum \quad space. \end{aligned} \tag{1.7}$$

1.3 Limiting Cases of the Bose-Hubbard Hamiltonian

1.3.1 Mott Insulating Phase

This limit corresponds to $\frac{t}{U} \to 0$, and the Bose-Hubbard Hamiltonian reduces to;

$$\hat{H}_{on-site} = \frac{U}{2} \sum_i \hat{n}_i \left(\hat{n}_i - 1\right) - \mu \sum_i \hat{n}_i \tag{1.8}$$

Hence, the ground state wavefunction is just the product state of single particles, which can be represented as [17];

$$|\Psi_{MI}> = \prod_i^{L^d} \left(\hat{b}_i^\dagger\right)^n |0> \tag{1.9}$$

where n is the boson per site, L is lattice site, and d is the dimensionality.

(1.8) is minimized for integer values of $n_0 = \frac{1}{2} + \frac{\mu}{U}$. As we have a commensurate fillings for a finite range of the chemical potential, we can say that the ground state, in this case, is incompressible, where compressibility is defined as $\kappa = \frac{\partial \rho}{\partial \mu}$ with ρ is the boson density [17].

As we consider the particle correlations in the ground state, we can realize that expectation value for such a correlation in momentum space, for practical reasons, i.e. $< \hat{b}_q^\dagger \hat{b}_q >$ is independent of the value q; meaning, we have a delocalization in momentum space as each momentum has the same weight; contrarily, we have localization in real space.

1.3.2 Superfluid Phase

This limit corresponds to $\frac{t}{U} \to \infty$, and the Bose-Hubbard Hamiltonian reduces to;

$$\hat{H}_{hopping} = -t \sum_{<i,j>} \left(\hat{b}_i^\dagger \hat{b}_j + h.c. \right) \tag{1.10}$$

Since, hopping term is diagonal in momentum space, we can further represent it as;

$$\hat{H}_{hopping} = \sum_{k_i} \hat{n}_{k_i} \epsilon(k_i) \quad with \quad \epsilon(k_i) = -2t \cos\left(k_i x_i\right) \tag{1.11}$$

For such a Hamiltonian, we cannot use the same ground state wavefunction anymore; however, we can define a new one as [18];

$$|\Psi_N>_{U=0} = \frac{1}{\sqrt{N!}} \left(\frac{1}{\sqrt{L!}} \sum_{\vec{x}} \hat{b}_{\vec{x}}^\dagger \right)^N |0> \tag{1.12}$$

Since all particles would occupy the possible lowest energy, ground state of the Hamiltonian would be at $k = 0$; meaning, particles are well localized in a single state with a coherent phase [17] in momentum space; whereas, they are delocalized in real space.

Observe that since the bosons, now, have coherent phase, particle number is allowed to fluctuate, which breaks the $U(1)$ symmetry as mentioned in Subsection.1.2. This broken-symmetry state is called *superfluid state*.

1.4 Outline of the thesis

In this thesis, our goal is to analyse one dimensional Bose-Hubbard model by using projected wavefunctions; i.e. namely *Baeriswyl*, and *Gutzwiller-Baeriswyl*, via variational Monte Carlo calculations. We examine the observables in forms of averages over configurations which we can apply MC techniques. Critical values of the Mott lobes existing in the phase diagrams for the two different variational wavefunctions, which we used in this thesis, are analysed and compared with each other, and also with a reference value [19]. Besides, we calculated the superfluid fraction with a new method [9,10] taking Drude weight as basis, apart from other known methods [5,6].

The thesis is organized as; in *Chapter 2*, some basic background and general definitions which are deeply related to the Bose-Hubbard model are given, in *Chapter 3*, both analytical and computational methods done so far are analysed basically, in *Chapter 4*, the algorithm we developed is introduced, and finally in the last chapter, results that we obtained from the projected wavefunctions are presented and compared.

Chapter 2

Background and General Definitions

2.1 Bose-Einstein Condensation

Consider a many-body wavefunction which is symmetric under exchange of pairs i and j; $\Psi\left(\vec{r_1},...,\vec{r_N}\right)$ where N is the number of bosons. The single-particle density matrix can be written as [20];

$$\begin{aligned}\rho_1\left(\vec{r},\vec{r'}\right) &\equiv N\sum_i p_i \int d\vec{r_2}...d\vec{r_N}\Psi_i^*(\vec{r},\vec{r_2},...,\vec{r_N})\Psi_i(\vec{r'},\vec{r_2},...,\vec{r_N}) \\ &\equiv <\hat{\Psi}^\dagger(\vec{r})\,\hat{\Psi}(\vec{r'})>\end{aligned} \tag{2.1}$$

where p_i is the probability of state i. Density matrix can be further expanded to include spin and time as well.

Since ρ_1 matrix is hermitian, i.e. $\rho_1(\vec{r},\vec{r'}) \equiv \rho_1^*(\vec{r'},\vec{r})$, we can diagonalise it in such a form [20];

$$\rho_1\left(\vec{r},\vec{r'}\right)=\sum_i n_i\chi_i^*(\vec{r})\chi_i(\vec{r'}) \tag{2.2}$$

where $\chi_i(\vec{r})$ forms an orthonormal set, and n_is are being the eigenvalues of this set.

Based on (2.2), we can give a formal definition of BEC as [20];

1. BEC does not occur if all the eigenvalues of (2.2) are of the order unity.
2. Simple BEC occurs if exactly one eigenvalue of (2.2) is of the order N and the rest of the eigenvalues are of the order unity.
3. Fragmented BEC occurs if two or more eigenvalues are of the order N and the rest of the eigenvalues are of the order unity.

BEC can be checked depending on the choice of the order parameter defining the condensate. Hence, I include the two different approaches to check the condensate.

First criterion for the BEC with an associated order parameter is based on using the boson field operators. The order parameter for this approach can be written as [20];

$$\psi\left(\vec{r}\right)\equiv<\hat{\psi}\left(\vec{r}\right)> \tag{2.3}$$

where $\hat{\psi}(\vec{r})$ is the boson field operator satisfying the commutation relations $\forall \vec{r}, \vec{r'}$;

$$\left[\hat{\psi}(\vec{r}), \hat{\psi}\left(\vec{r'}\right)\right] = \left[\hat{\psi}^{\dagger}(\vec{r}), \hat{\psi}^{\dagger}\left(\vec{r'}\right)\right] = 0 \tag{2.4}$$

$$\left[\hat{\psi}(\vec{r}), \hat{\psi}^{\dagger}\left(\vec{r'}\right)\right] = \delta\left(\vec{r} - \vec{r'}\right) \tag{2.5}$$

Note that the order parameter, i.e. $\hat{\psi}(\vec{r})$ can be expanded to include time as well.

In order for BEC to occur, in the limit $\left|\vec{r} - \vec{r'}\right| \to \infty$, right hand side of the (2.2) must have a value different than zero [20].

Second criterion for the BEC with an associated order parameter, on the other hand, based on including density and phase terms. The order parameter for this approach can be written as [20];

$$\psi(\vec{r}) \equiv \sqrt{N_0}\chi_0(\vec{r}) \tag{2.6}$$

Obeying the normalization condition;

$$\int d\vec{r}|\psi(\vec{r})|^2 = N_0 \tag{2.7}$$

where $\chi_0(\vec{r})$ is a single-particle wavefunction which is orthonormal and can be defined as [20];

$$\chi_0(\vec{r}) \equiv |\chi_0(\vec{r})|e^{i\varphi(\vec{r})} \tag{2.8}$$

where $\varphi(\vec{r})$ is the phase of the condensate, i.e. $\chi_0(\vec{r})$, wavefunction.

To check the BEC in this approach, one can use the single-particle density matrix in the limit $|\vec{r}-\vec{r'}| \to \infty$ [20];

$$\lim_{|\vec{r}-\vec{r'}|\to\infty} \rho_1\left(\vec{r},\vec{r'}\right) = f^*\left(\vec{r}\right) f\left(\vec{r'}\right) + \tilde{\rho_1}\left(\vec{r},\vec{r'}\right) \tag{2.9}$$

In the limit $|\vec{r}-\vec{r'}| \to \infty$, $\tilde{\rho_1}\left(\vec{r},\vec{r'}\right) \to \infty$ and $f\left(\vec{r}\right)$ goes to a non-zero value if the condensate occurs [20].

2.2 Superfluid Phase

In 1938, two different groups (Kapitsa in Moscow, and Allen Misener in Cambridge) simultaneously realized a peculiar behaviour of ^4He below the λ-point, i.e. $\simeq 2.17$K. They observed that the liquid flowed easily without friction through a narrow channel between two bulk reservoirs [20, 21]. This behavior was later labeled as *superfluid* by Kapitsa.

The more clear and modern definition of superfluidity, on the other hand, can be understood via observing two conceptually different cases, which can also be called as *generalized BEC* [20]. These two cases are considered on a multiply connected geometry, e.g. annular region between two concentric cylinders, unlike the narrow channel between two bulk reservoirs.

Due to the fact that superfluid velocity is not a directly measurable quantity, it is suitable to define another quantity in which one can track the existence or the absence of superfluid phase, i.e. *current density* [20];

$$\vec{J}\left(\vec{r}\right) = \rho_s\left(\vec{r}\right)\vec{v}_s\left(\vec{r}\right) + \rho_n\left(\vec{r}\right)\vec{v}_n\left(\vec{r}\right) \tag{2.10}$$

where ρ_n is normal fluid density, whereas ρ_s superfluid density, and $\vec{v}_n$ is normal fluid velocity, whereas $\vec{v}_s$ superfluid velocity.

This is actually called the two fluid model, and it can be explained with hydrodynamic equations

Two give a full picture of the phenomena, one needs to define another condition in which phase of the condensate wavefunction is also included. For the spinless case (it can be written for the spinfull case as well) candensate wavefunction can be written as [20];

$$\chi_0\left(\vec{r},t\right) \equiv |\chi_0\left(\vec{r},t\right)|e^{i\varphi(\vec{r},t)} \tag{2.11}$$

Hence, the current carried by condensate;

$$\vec{J}\left(\vec{r},t\right) \equiv N_0|\chi_0\left(\vec{r},t\right)|^2\frac{\hbar}{m}\vec{\nabla}\varphi\left(\vec{r},t\right) \tag{2.12}$$

where N_0 is number of particles in the condensate.

Note that the ratio $\frac{J(\vec{r},t)}{\rho(\vec{r},t)}$ has the dimensions of velocity which is defined as *superfluid velocity* [20];

$$\vec{v}_s\left(\vec{r},t\right) \equiv \frac{\hbar}{m}\vec{\nabla}\varphi\left(\vec{r},t\right) \tag{2.13}$$

With the condition that $\chi_0\left(\vec{r},t\right)$ has a non-zero value, $\vec{v}_s$ satisfies [20];

1. Irrotationality:

$$\vec{\nabla} \times \vec{v}_s(\vec{r}, t) = 0 \tag{2.14}$$

2. Onsager-Feynman quantization:

$$\oint_C d\vec{l} \cdot \vec{v}_s(\vec{r}, t) = \frac{nh}{m} \tag{2.15}$$

where n is an integer and also called *winding number*.

Hence, the more clear definition for superfluid phase, accepting the multiply connected geometry, now, can be explained with two cases as mentioned [20];

1. Hess-Fairbank Effect:
   While an annulus is being rotated with an angular velocity ω, cool the system down to the λ-point, and wait for the system to reach thermal equilibrium. Since the temperature is above the λ-point, Helium will behave like a normal liquid. Hence, the current density will be $\propto \rho\vec{v}_n$ with $\vec{v}_n = \vec{\omega} \times \vec{r}$, and the angular momentum is $\vec{L} = I_{classical}\vec{\omega}$.

   Now, cool the system down below the λ-point. One expects to see another phase; i.e. He-II [20, 21], the superfluid phase. Due to the Onsager-Feynman quantization condition, (2.15), we have discrete values for v_s, i.e. $v_s = n\omega_c R$, where n is the winding number defined in (2.15).

   The value of n in which the system prefers can be determined by minimizing the effective energy [20];

$$\hat{H}_{eff} \equiv \hat{H}_{lab} - \vec{\omega} \cdot \hat{\vec{L}} \tag{2.16}$$

   where the annulus is stationary in lab frame, which is given by;

$$\hat{H}_{lab} = \sum_i \left(\frac{p_i^2}{2m} + V_{ext}(\vec{r}_i) \right) + \frac{1}{2} \sum_{i,j} U(|\vec{r}_i - \vec{r}_j|) \tag{2.17}$$

Minimization of $\hat{H}_{eff}$ gives an expression depending on the winding number [20];

$$\varepsilon = \rho_s(\vec{r})\, R^2 \left(\frac{1}{2} n^2 \omega^2 - n\omega\omega_c \right) \tag{2.18}$$

This expression is further minimized with respect to n by choosing n as integer values of the ratio $\frac{\omega}{\omega_c}$, i.e. $n \simeq int\left(\frac{\omega}{\omega_c}\right)$ [20]. Contribution of superfluid and normal components to the total angular momentum can be identified depending on which value that ω chooses, i.e. [20];

(a) For $\omega < \frac{\omega_c}{2}$; $\vec{v}_s = 0$ and the total angular momentum is reduced by a factor $\frac{\rho_n}{\rho} \equiv g_n(T)$ with $L(T) = g_n(T)\, I_{classical}\omega$.

(b) For $\omega > \frac{\omega_c}{2}$; $\vec{v}_s \neq 0$ and the total angular momentum is reduced by $\frac{\rho_s}{\rho} \equiv g_s(T)$ with superfluid contribution to the above equation to the angular momentum is $L(T) = g_s(T)\, I_{classical} n\omega_c$.

Hence, the total angular momentum is [20];

$$L(T) = \left[g_n(T)\, \omega + g_s(T)\, n\omega_c \right] I_{classical} \tag{2.19}$$

with $n \equiv int\left(\frac{\omega}{\omega_c} + \frac{1}{2}\right)$.

2. Metastability of Supercurrents:

This time the annulus is being rotated with a much larger angular velocity $\omega_0 \equiv \omega \gg \omega_c$ [20]. Again, cool the system down to the λ-point. v_s, by the Onsager-Feynman constraint, will take quantized values which are close to $int\left(\frac{\omega_c}{\omega}\right)$. However, the value of v_s, due to $\omega_0 \gg \omega_c$, should be so small that any contribution made by the superfluid component will be small and angular momentum would be only $L(T) \simeq I_{classical}\omega_0$.

If we further cool the system down below the λ-point, and stop the rotation of the annulus, $v_n = 0$, but superfluid component persist for a while, then, $n \equiv int\left(\frac{\omega_0}{\omega_c} + \frac{1}{2}\right)$ and, hence, the angular momentum is [20];

$$L(T) \simeq g_s(T)\,\omega_0 I_{classical}. \tag{2.20}$$

That is even though it is not the equilibrium one, system has a persistent superfluid circulation which leads to metastable superflow.

In order to determine the superfluid fraction, one needs to consider the system response to the boundary condition. It can, basically, be measured either by calculating the free energy change in a periodic system which is based on winding number calculation or by calculating the momentum-density correlation function [5].

1. Winding number Approach:
   This approach is based on calculating the density matrix for the moving walls, i.e. rest frame for the walls; ρ_v [5];

$$\rho_v = e^{-\beta \hat{H}}, \qquad \hat{H} = \sum_i \frac{(\vec{p}_i - m\vec{v})^2}{2m} + V \tag{2.21}$$

   where V is the interaction potential.

   Response of the fluid to the boundary motion can be written in terms of the total momentum operator, $\vec{P}$ [5];

$$< \vec{P} >_v = \frac{\rho_n}{\rho} N m \vec{v} = \frac{Tr\left\{\vec{P}\rho_v\right\}}{Tr\left\{\rho_v\right\}} \tag{2.22}$$

   where ρ_n is the normal component of the fluid.

   This equation can also be written with respect to the superfluid fraction [5];

$$\frac{\rho_s}{\rho} = \frac{\partial\left(F_v/N\right)}{\partial\left(\frac{1}{2}mv^2\right)} \tag{2.23}$$

where F_v is the free energy, and free energy change can be computed as [5];

$$\frac{\triangle F_v}{N} = \frac{1}{2} m v^2 \frac{\rho_s}{\rho} + O\left(v^4\right). \tag{2.24}$$

Note that by (2.21), the density matrix satisfies the Bloch equation, hence, obey the periodic boundary condition requirement which brings a phase factor in front of the density matrix coming from the path ending as [5]; $e^{i\frac{m}{\hbar}\vec{v}\cdot\vec{L}}$.

This factor introduces the so called *winding number*, W [5];

$$\sum_{j=1}^{N} \left(\vec{r'}_j - \vec{r}_j\right) = \vec{W} L \tag{2.25}$$

where $\vec{r}_j$ is the initial point and $\vec{r'}_j$ is the destination point.

Free energy change can be calculated by using the winding number [5];

$$e^{-\beta \triangle F_v} = \frac{\int d\vec{r} \rho_{\vec{v}}\left(\vec{r}, \vec{r}; \beta\right)}{\int d\vec{r} \rho_{\vec{v}=0}\left(\vec{r}, \vec{r}; \beta\right)} =< e^{i\frac{m}{\hbar}\left(\vec{v}\cdot\vec{W}L\right)} > \tag{2.26}$$

By using the $\frac{\triangle F_v}{N}$ expansion in (2.24), for small velocities, the above relation can be written for a d-dimensional system as [5];

$$\frac{\rho_s}{\rho} = \frac{m}{\hbar^2} \frac{< W^2 > L^{2-d}}{\rho d \beta} \tag{2.27}$$

2. Momentum-Density Correlation Function Approach:

   This approach is based on the momentum response of the fluid to the boundary motion. For a system having periodic boundary conditions, only the normal component of the fluid responds, and hence, expanding (2.22) to the first order in v gives [5];

$$\frac{\rho_n}{\rho} N m \vec{v} =< \vec{P} >_v = \beta < \vec{P}\vec{P} > \cdot \vec{v} \tag{2.28}$$

   In terms of momentum density, i.e. $\vec{p}(\vec{r})$, (2.28) can be written as [5];

$$< \vec{p}(\vec{r}) >_v = \beta \int_{over \quad all \quad volume} d^3 r' \vec{v} \cdot < \vec{p}(\vec{r})\, \vec{p}\left(\vec{r'}\right) >_{v=0} \tag{2.29}$$

   In an isotropic liquid, the normal component of the fluid can be written in terms of momentum density correlation function as [5];

$$\rho_n = \frac{\beta}{3m} \int d^3 r < \vec{p}(\vec{r}) \cdot \vec{p}(0) > \tag{2.30}$$

3. Single-Particle Delocalization Approach:

   Apart from previously used techniques, there is another way to detect the existence of superfluid phase based on *Drude weight*.

   This approach is based on the Drude weight expression which was basically introduced to distinguish metals from insulators, and can be expressed in the form [7, 8];

$$D_c = \frac{\pi}{V} \left[\frac{\partial^2 E(\phi)}{\partial \phi^2} \right]_{\phi=0} \tag{2.31}$$

   where E is the ground state energy and ϕ is the phase introduced as perturbation.

Based on (2.31), a more general relation can be written for the second order derivative of the ground state energy as [10];

$$\begin{aligned}\left[\frac{\partial^2 E(\phi)}{\partial\phi^2}\right]_{\phi=0} &= i\sum_{j=1}^{N} <\Psi|\left[\partial_{k_j},\partial_{x_j}\right]|\Psi> \\ &- \lim_{\triangle X,\triangle K\to 0}\frac{1}{\triangle X\triangle K}[Im\left\{ln\left(\frac{<\Psi|e^{i\triangle K\hat{X}}e^{i\triangle X\hat{K}}|\Psi>}{e^{i\triangle X\hat{K}}}\right)\right\} \\ &+ Im\left\{ln\left(\frac{<\Psi|e^{i\triangle X\hat{K}}e^{-i\triangle K\hat{X}}|\Psi>}{e^{i\triangle X\hat{K}}}\right)\right\}]\end{aligned} \tag{2.33}$$

where $\hat{K}=\sum_{j=1}^{N}\hat{k}_i$ and $\hat{X}=\sum_{j=1}^{N}\hat{x}_i$, with $\hat{k}_i$ and $\hat{x}_i$ are single momentum and position operators for each particle respectively.

In order to observe the existence of superfluid phase, (2.33) can be used in terms of the sum over expectation values of single momenta, and after taking the limit indicated, one can obtain [9, 10, 22, 23];

$$\sigma_x^2=-\frac{2}{(\triangle K)^2}Re\left\{ln\left(<\Psi|e^{-i\triangle K\hat{X}}|\Psi>\right)\right\} \tag{2.34}$$

If the wavefunction is an eigenstate of the one-body position shift operator, i.e. $e^{-i\triangle K\hat{X}}$, then, this expression contributes to the superfluid weight with a finite value [10, 24].

Chapter 3

Bose Hubbard Methods

3.1 Analytical Approach

3.1.1 Mean-Field Theory

Within a correlated system, the motion of each individual particle depends on all the others. To simplify such a system, a physical model is introduced in which correlations between the particles are not entirely included, but, instead, they are included on average. Hence, the effect of the other particles is introduced as mean-field, and the model can be treated as a single particle model.

Mean-field Hamiltonian, i.e. $\hat{H}_{MF}$, for the Bose-Hubbard model can be introduced as [15];

$$\hat{H}_{MF} = \sum_i \left(-\psi_B^* \hat{b}_i - \psi_B \hat{b}_i^\dagger \right) + \frac{U}{2} \sum_i \hat{n}_i \left(\hat{n}_i - 1 \right) - \mu \sum_i \hat{n}_i \tag{3.1}$$

where ψ_B is a variational operator. $\hat{b}_i^\dagger$, $\hat{b}_i$ are boson creation and annihilation operators respectively. $\hat{n}_i = \hat{b}_i^\dagger \hat{b}_i$ is the number operator which gives the number of particles on site i. U is the on-site interaction potential and μ is the chemical

potential.

The variational operators in (3.1) represent the neighboring effects, and they break the U(1) symmetry; hence, phase due to the broken-symmetry is introduced as *superfluid phase* [15].

In order to approximate the ground state energy of the BHM, a suitable ground state wavefunction must be introduced with an optimum value for the variational operator which minimizes the ground state energy.

Since we can consider the model as a single particle problem, a suitable ground state wavefunction is simply the product of single-site wavefunctions, and hence the ground state energy is [15];

$$\frac{E_0}{L} = \frac{E_{MF}\left(\psi_B\right)}{L} - zJ < \hat{b}^\dagger >< \hat{b} > + < \hat{b} > \psi_B^* + < \hat{b}^\dagger > \psi_B \tag{3.2}$$

where z is the coordination number, and L is the lattice site, with an optimum value $\psi_B = zJ < \hat{b} >$ [15].

Basically, three limits can be applied to the Hamiltonian;

1. J=0 (ψ_B=0):
   For this case, since the variational operator is excluded, sites become decoupled which gives exact result for the MFT [15]. The Hamiltonian contains only the number operator, thus, the problem is reduced to find only these boson occupation numbers which minimizes the Hamiltonian.

   Since $\hat{n}$ is a good quantum number, ground state wavefunction can be represented by these occupation numbers $|m_i = n_0 \left(\frac{\mu}{U}\right) >$ where n_0 is [15];

$$n_0\left(\frac{\mu}{U}\right) = \begin{cases} 0, & \frac{\mu}{U} < 0 \\ 1, & 0 < \frac{\mu}{U} < 1 \\ \vdots & \\ n, & n-1 < \frac{\mu}{U} < n \end{cases} \tag{3.3}$$

2. J$\neq$ 0 but small:
   For this case, since perturbation commutes with the Hamiltonian, system will evolve having exactly the same eigenvalues with the adiabatic increase of J. Hence, the exact result would be [15];

$$< \hat{b}_i^\dagger \hat{b}_i >= n_0\left(\frac{\mu}{U}\right) \tag{3.4}$$

   This result is responsible for the island existing in the phase diagram which are called as *Mott insulators* [15]. This phase is incompressible with $\frac{\partial < N >}{\partial \mu} = 0$.

3. J$\neq$ 0 ($\psi_B \neq 0$):
   For this case, ground state is delocalized over the lattice. Hence, one cannot use the same ground stated as indicated in (3.3), but, instead, can use [18];

$$|\Psi_N >_{U=0} = \frac{1}{\sqrt{N!}} \left(\frac{1}{\sqrt{L!}} \sum_{\vec{R}} \hat{a}^\dagger_{\vec{R}} \right)^N |0> \tag{3.5}$$

   Since the particle density does not take quantized values, it can change with μ, i.e. $\frac{\partial < N >}{\partial \mu} \neq 0$ which defines compressibility [15].

To determine the phase boundaries; as the variational operator, ψ is increased continuously, numerical analysis shows that the Mott insulator phase is a second order phase transition which can be explained using Landau theory [15]. Expansion of the ground state energy with respect to ψ gives [15];

$$E_0 = E_{00} + r|\psi|^2 + O\left(|\psi|^4\right)^* \tag{3.6}$$

where the coefficient r can be found by using the second order perturbation theory [15];

$$r = \Gamma_0 \left(1 - zJ\Gamma_0\right) \tag{3.7}$$

where Γ_0 is

$$\Gamma_0 = \left(\frac{n_0\left(\frac{\mu}{U}\right) + 1}{Un_0\left(\frac{\mu}{U}\right) - \mu} + \frac{n_0\left(\frac{\mu}{U}\right)}{\mu - U\left(n_0\left(\frac{\mu}{U}\right) - 1\right)} \right) \tag{3.8}$$

For r=0, phase boundary is found.

3.1.2 Perturbative Methods

The perturbative method is another way to treat the Bose-Hubbard Hamiltonian. With this method, one can use either strong or weak coupling approaches. In this thesis, strong coupling approach is covered based on the calculations of Freericks [25].

For the strong coupling limit, kinetic energy vanishes and each site has a fixed number of bosons; n_0.

For such a system, let the chemical potential to be parametrized as [25]; $\mu = (n_0 + \delta)\, U$ where n_0 is ground state boson occupancy, and δ is the deviation from integer filling.

The phase boundary between the Mott insulator and superfluid phases can be

determined by calculating the energy of the Mott insulator phase and the defect phase, which occurs due to adding hole ($\delta > 0$) or particle ($\delta < 0$) to the system [25], and then, treating the kinetic energy term perturbatively.

Based on the two cases for the defect phase, i.e. $\delta > 0$ and $\delta < 0$, one needs to calculate three different relations: E_{MI}, $E_{defect}^{\delta>0}$, $E_{defect}^{\delta<0}$ to determine the phase boundary.

Relevant wavefunctions which are to the zeroth order in $\frac{t}{U}$ for calculating the energy relations are given as [25];

1. Wavefunction which belongs to the Mott insulator phase:

$$|\Psi_{Mott}\left(n_0\right)>^{(0)}=\prod_{i=1}^{N}\frac{1}{\sqrt{n_0!}}\left(\hat{b}_i^{\dagger}\right)^{n_0}|0> \tag{3.9}$$

2. Wavefunction which belongs to the particle for defect phase:

$$|\Psi_{Def}\left(n_0\right)>_{(\delta<0)}^{(0)}=\frac{1}{\sqrt{n_0+1}}\sum_i f_i\hat{b}_i^{\dagger}|\Psi_{Mott}\left(n_0\right)>^{(0)} \tag{3.10}$$

3. Wavefunction which belongs to the particle for defect insulator phase:

$$|\Psi_{Def}\left(n_0\right)>_{(\delta>0)}^{(0)}=\frac{1}{\sqrt{n_0}}\sum_i f_i\hat{b}_i|\Psi_{Mott}\left(n_0\right)>^{(0)} \tag{3.11}$$

where N is the number of sites in lattice, f_i is the eigenstate of the hopping matrix t_{ij} with the lowest eigenvalue.

Energy differences to the third order in $\frac{U}{t}$ between the Mott insulator and defect phases are given as [25];

1. For an extra particle:

$$\begin{aligned} E_{Def}^{(\delta<0)}(n_0) - E_{Mott}(n_0) &= -\delta^{(particle)}U - zt(n_0+1) \\ &+ \frac{zt^2}{U}\frac{n_0(5n_0+4)}{2} - \frac{z^2t^2}{U}n_0(n_0+1) \\ &+ \frac{t^3}{U^2}n_0(n_0+1)\left[\left(-2z^3+\frac{25}{4}z^2-4z\right)n_0\right. \\ &+ \left.\left(-z^3+\frac{7}{2}z^2-2z\right)\right] \end{aligned} \tag{3.12}$$

2. For an extra hole:

$$\begin{aligned} E_{Def}^{(\delta>0)}(n_0) - E_{Mott}(n_0) &= \delta^{(hole)}U - ztn_0 \\ &+ \frac{zt^2}{U}\frac{(n_0+1)(5n_0+1)}{2} - \frac{z^2t^2}{U}n_0(n_0+1) \\ &+ \frac{t^3}{U^2}n_0(n_0+1)\left[\left(-2z^3+\frac{25}{4}z^2-4z\right)n_0\right. \\ &+ \left.\left(-z^3+\frac{11}{4}z^2-2z\right)\right] \end{aligned} \tag{3.13}$$

where

$$E_{Mott}(n_0) = N\left[-\delta U n_0 - \frac{1}{2}Un_0(n_0+1) - \frac{zt^2}{U}n_0(n_0+1)\right] \tag{3.14}$$

Phase boundary between the Mott insulator phase and the superfluid phase can be found by setting the energy difference to zero where these two branches meet at [25]; $\delta^{(particle)}(n_0)+1 = \delta^{(hole)}(n_0)$.

Hence, upper and lower boundaries of the Mott insulator lobe in one dimension are given as [25];

1. Upper boundary:

$$\delta^{(particle)}\left(n_0, \frac{t}{U}\right) = -2\left(n_0+1\right)\left(\frac{t}{U}\right) + n_0^2\left(\frac{t}{U}\right)^2 + n_0\left(n_0+1\right)\left(n_0+2\right)\left(\frac{t}{U}\right)^3 \tag{3.15}$$

2. Lower boundary:

$$\delta^{(hole)}\left(n_0, \frac{t}{U}\right) = 2n_0\left(\frac{t}{U}\right) - \left(n_0+1\right)^2\left(\frac{t}{U}\right)^2 + n_0\left(n_0+1\right)\left(n_0-1\right)\left(\frac{t}{U}\right)^3 \tag{3.16}$$

A similar approach can be done for weak coupling limit.

3.2 Computational Approach

Dealing with the physics of many-body systems consisting of a large number of interacting particles is in general difficult. Finding an exact solution for such systems as the dimensionality and the total particle number increases becomes impossible. Therefore, a suitable computational approach to such systems is necessary.

In this section, most common computational approaches to the many-body systems are discussed.

3.2.1 Exact Diagonalisation Method

In order to find the eigenvalues of a n-dimensional many-body Hamiltonian one needs to solve a characteristic polynomial with degree n in which finding an exact solution is not possible for n>4 [26].

To be more quantitative, for Hubbard model, in general, with N particles there are 4^N states. This brings a limitation on the lattice site as it costs computer time and memory. For instance for the ultra-cold atom systems $L \cong 22 - 25$, for square lattice at half-filling it is $L \cong 20$, and for the triangular lattice $L \cong 21$ [27]. Thus the exponential growth of the matrix $\hat{H}$ even with small lattice sites makes it hard to calculate the eigenvalues with the usual diagonalisation methods. One suggestion to this problem is that by using the symmetries of the model, one can find a unitary transformation which has the same characteristic polynomial, i.e. $\hat{H} \to U^\dagger \hat{H} U$, and find its eigenvalues instead.

It is necessary to construct the U matrix in an iterative way until the matrix $\hat{H}$ becomes diagonal, i.e. $\hat{H} \to U_1^\dagger \hat{H} U_1 \to U_2^\dagger U_1^\dagger \hat{H} U_1 U_2 \to ...$ In order to diagonalise the Hamiltonian Lanczos type algorithms can be used. To do this, one should choose a convenient basis function first and then recursively produce new states until the ground state energy is converged.

As for the low temperature systems, the most relevant eigenstates are either the ground state or the lowest lying excited states. Thus, the initial random choice of state can be chosen with a finite overlap with the ground state. That is [28]

$$|\psi_{m+1}> = \hat{H}|\psi_m> - \alpha_m|\psi_m> - \beta_m^2|\psi_{m-1}> \tag{3.17}$$

with coefficients;

$$\alpha_m = \frac{<\psi_m|\hat{H}|\psi_m>}{<\psi_m|\psi_m>} \qquad \beta_m^2 = \frac{<\psi_m|\psi_m>}{<\psi_{m-1}|\psi_{m-1}>} \tag{3.18}$$

Then, as a final step, diagonalise the obtained sparse matrix.

With the exact diagonalisation method, one can calculate static quantities like correlation functions or dynamical quantities like density of states.

3.2.2 Quantum Monte Carlo Method

Dealing with quantum systems is more difficult than dealing with the classical systems because in the former case one does not know the exact distribution which is to be sampled however one knows the exact Hamiltonian to be solved.

QMC methods are generally based on a random walk process. Simulation starts with a random but reasonable configuration of the system. Then, probability of each configuration is calculated based on Metropolis algorithm, which will be covered in Chapter-4 in detail. With the help of this algorithm, one extracts the 'good' probabilities, i.e. accepted ones which lead convergent expectation values, and is able to calculate the mean values for the physical system.

Except for the projection method algorithm, which will be covered in Chapter-4 in detail, the most common algorithms which constitute the basis of QMC simulations are 'Discrete-time world-line algorithm' and 'Stochastic series expansion algorithm'.

3.2.2.1 Discrete-Time World-Line Algorithm

This algorithm is based on the path integral formulation of the partition function in imaginary time. The aim is to compute the physical observables either in the canonical ensemble or in the grand canonical ensemble.

The core idea is to use the Suzuki-Trotter decomposition. For the case of a 1 dimensional system, when only nearest neighboring site coupling is allowed, i.e. $\left[\hat{H}_{i,i+1}, \hat{H}_{j,j+1}\right] = 0 \quad where \quad j > i+1$. Thus, one can split $\hat{H}$ into even and odd terms like $\hat{H} = \hat{H}_{even} + \hat{H}_{odd}$ and expand the partition function as [29, 30];

$$
\begin{aligned}
Z &\simeq Tr\left\{\prod_{n=1}^{L} e^{-\Delta\tau\hat{H}_{even}} e^{-\Delta\tau\hat{H}_{odd}}\right\} \\
&= \sum_{n_1,\ldots,n_{2L}} < n_1|exp\left(-\Delta\tau\hat{H}_{even}\right)|n_{2L}>< n_{2L}|exp\left(-\Delta\tau\hat{H}_{odd}\right)|n_{2L-1}> \\
&\ldots \; < n_3|exp\left(-\Delta\tau\hat{H}_{even}\right)|n_2>< n_2|exp\left(-\Delta\tau\hat{H}_{odd}\right)|n_1>
\end{aligned}
\tag{3.19}
$$

where L is the lattice site, $\Delta\tau = \frac{\beta}{L}$ is the imaginary time, and $\{|n_i>\}$ is the complete basis set for each imaginary time interval.

This decomposition leads to a checkerboard picture of space-time to track the movements of particles along the world-lines which are moved via local updates [31]. However, the Suzuki-Trotter decomposition brings an error term on the order $O(\Delta\tau^2)$. In order to overcome this error, one needs to introduce the continuous time limit, i.e. $\Delta\tau \to 0$, [32, 33];

$$
\begin{aligned}
Z &= Tr\left\{e^{-\beta\hat{H}}\right\} \\
&= Tr\left\{e^{-\beta\hat{H}_D} e^{-\int_0^\beta d\tau \hat{H}_{OD}(\tau)}\right\} \\
&= Tr\left\{e^{-\beta\hat{H}_D}\left(1 - \int_0^\beta d\tau \hat{H}_{OD}(\tau) + \frac{1}{2}\int_0^\beta d\tau_1 \int_{\tau_1}^\beta d\tau_2 \hat{H}_{OD}(\tau_1)\hat{H}_{OD}(\tau_2) + \ldots\right)\right\}
\end{aligned}
\tag{3.20}
$$

where D stands for diagonal and OD stands for off-diagonal with $\beta = \frac{1}{k_B T}$.

Note that in the interaction representation, one can write the time-dependent off-diagonal Hamiltonian as $\hat{H}_{OD}(\tau) = e^{\tau\hat{H}_D}\hat{H}_{OD}e^{-\tau\hat{H}_D}$.

However, still, such local updates on the checkerboard picture do not change the global properties like number of world lines as a cost of using canonical ensemble. In order to use grand canonical ensemble, global updates must be introduced with the so called *loop algorithm* [34] and its continuous time limit version [35].

3.2.2.2 Stochastic Series Expansion

This algorithm is based on power-series expansion of the partition function [36];

$$\begin{aligned} Z &= Tr\left\{e^{-\beta\hat{H}}\right\} \\ &= \sum_{n=0}^{\infty}\frac{\beta^n}{n!}Tr\left(-\hat{H}\right)^n \\ &= \sum_{n=0}^{\infty}\frac{\beta^n}{n!}\sum_{\{m_1,\ldots,m_n\}}\sum_{\{b_1,\ldots,b_n\}} < m_1|-\hat{H}_{b_1}|m_2 >< m_2|-\hat{H}_{b_2}|m_3 > \ldots < m_n|-\hat{H}_{b_n}|m_1 > \end{aligned} \tag{3.21}$$

where b is the bond index. Note that one can obtain (3.5) by setting $\hat{H}_D = 0$ and $\hat{H}_{OD} = \hat{H}$ in (3.4).

As it is seen from (3.4) and (3.5) that in world-line algorithm only the off-diagonal is treated as perturbation series whereas in stochastic series expansion whole Hamiltonian is treated as perturbation series. In practice SSE is preferred because in continuous world-line algorithms, one has to deal with the high-precision values of the imaginary time [37].

3.2.3 Density Matrix Renormalization Group Method

DMRG, which was developed by S. R. White [38,39], is based on an iterative and also a variational method in which only the most significant states are considered. The aim is to divide the system into blocks and treat every block separately. While doing this, the interactions among the blocks must also be considered.

Starting point for DMRG is the block renormalization which follows the steps basically [40];

Let n $\equiv$ number of states in a block.

1. Create an initial block-A, i.e. $\hat{H}_A$ with length l acting on an n-dimensional Hilbert space.

2. Then, create a compound block-AA, i.e. $\hat{H}_{AA}$ with length 2l. The compound block Hamiltonian consists of two block Hamiltonians which has dimensionality = n^2.

3. Diagonalise $\hat{H}_{AA}$ and find the n lowest-lying eigenvectors.

4. Project $\hat{H}_{AA}$ on the truncated space which is spanned by n lowest-lying eigenvectors, i.e. $\hat{H}_{AA} \rightarrow \hat{H}'_{AA}$

5. Start from 2l $\rightarrow$ l and $\hat{H}'_{AA} \rightarrow \hat{H}_A$. Till the lattice site is reached.

In this method, blocks are considered as independent systems and each block has its own boundary condition. When these blocks are combined same boundary conditions for each block cannot be applied this time as it will not give the true ground state [41]. Thus, instead of just calculating the ground state of the block itself, one should consider the ground state of the compound system and the environment, i.e. *super-block*, and after finding the ground state of the super-block, found state is mapped on the block and the block space is truncated with the following formulation [41];

Compound system state can be written as;

$$|\Psi> = \sum_{i,j} \lambda_{ij} |\alpha_i> \otimes |\beta_j> \tag{3.22}$$

where $|\alpha_i>$ is a state in block space and $|\beta_j>$ is a state in environment space.

As a next step, environment is traced out and the density matrix for the block only is calculated;

$$< \alpha_i^{'} | \rho_{Block} | \alpha_i > = \sum_j \lambda_{ij}^* \lambda_{i^{'}j} \tag{3.23}$$

Note that the density matrix, i.e. ρ_{Block}, must be;

1. Self-adjoint: $\rho^{\dagger} = \rho$,
2. Semi-positive definite: $\rho \geq 0$,
3. Tracing out to unity: $Tr\{\rho\} = 1$.

The goal is to find the states which have highest eigenvalues so that the ground state of the super-block is described properly.

Clear definition of steps can be summarized as;

Define m $\equiv$ number of states in a block and n $\equiv$ number of states on a site.

1. Introduce left and right Hamiltonians; i.e. $\hat{H}_L$ and $\hat{H}_R$ acting on an m-dimensional Hilbert space.
2. Introduce the interactions as left-center and right-center; i.e. $\hat{H}_{LC}$ and $\hat{H}_{RC}$.
3. Then, introduce the super-block Hamiltonian; $\hat{H}_{SB}$ which is consist of $\hat{H}_L$, $\hat{H}_R$, $\hat{H}_{LC}$, and $\hat{H}_{RC}$ with dimensionality $= m^2n^2$.
4. Diagonalise $\hat{H}_{SB}$ and find the ground state.
5. Calculate ρ_{Block} for left and also for right part.
6. Calculate the m-eigenvectors having the highest eigenvalues for left and also for right part.
7. Map left part Hamiltonian; i.e. $\hat{H}_L$, $\hat{H}_{LC}$. on m-dimensional truncated space spanned by the eigenstates which are found in step-6, and do it for the right part of Hamiltonian as well.

There are two types of DMRG; one being the infinite-size DMRG and the other is finite-size DMRG. For further details one can check [41].

DMRG is one of the good and powerful technique for one dimensional problems as the method is based on a low-entanglement approximation. Thus, it is usually preferred to obtain exact solutions in one dimensional.

Chapter 4

Algorithm

4.1 Variational Monte Carlo Method

Quantum Monte Carlo methods allow to calculate expectation values with the help of stochastic sampling by using the so called Metropolis algorithm [42]. This algorithm generates Markov chains, i.e. random walks, over a configuration space. Each configuration is sampled based on a stationary probability distribution.

VMC, on the other hand, is one of the QMC methods in which Metropolis algorithm is directly used to describe the ground state properties of the system stochastically based on a suitable trial wavefunction.

As a historical side note, VMC method was first applied to a bosonic many-body system to observe the ground state properties of the ^4He [43], and, it was applied to the Hubbard model [44] by introducing the celebrated Gutzwiller wavefunction, and the final basic contribution is done by using the square of an anti-symmetric wavefunction to sample the configuration space as an equivalent approach for fermionic many-body problems rather than bosonic ones [45, 46].

4.1.1 Metropolis-Hastings Algorithm

The basic idea of this algorithm is to sample over the configuration space based on acceptance or rejection criteria but keep only the good samples. Applying this idea to the VMC leads to an algorithm based on the following steps;

1. Choose a set of coordinates in the Markov chain; $\{x_i\}^j$ randomly (or from the obtained set from previous configuration).

2. Then, suggest a move with a trial set of coordinates; $\left\{x_i^{'}\right\}^j$. The probability of accepting the move is

$$P = min\left[1, \left|\frac{\psi\left\{x_i^{'}\right\}^j}{\psi\left\{x_i\right\}^j}\right|^2\right] \tag{4.1}$$

   where $\psi\left\{x_i\right\}^j$ is the variational wavefunction of the system with a configuration $\{x_i\}^j$.

3. Generate a random number r st. $0 < r \leq 1$.

4. If $\left|\frac{\psi\left\{x_i^{'}\right\}^j}{\psi\{x_i\}^j}\right|^2 \geq r$, accept the move: $\{x_i\}^{j+1} = \left\{x_i^{'}\right\}^j$.

   Else, reject the move: $\{x_i\}^{j+1} = \{x_i\}^j$.

5. Then, suggest a new move (step-2) and repeat the process.

Based on the central limit theorem, for large enough samplings, average quantities calculated with the Metropolis algorithm give reliable estimates of the expectation values.

4.2 Adaptation of the VMC Method to the Bose-Hubbard Model

The following derivations can be applied to any dimension; however, in this thesis results are obtained for a one dimensional system only.

We adapated VMC to the BHM with two different variational wavefunctions, namely; the *Baeriswyl* and *Gutzwiller-Baeriswyl* variational wavefunctions.

4.2.1 Baeriswyl Projection

Baeriswyl variational wavefunction is defined as;

$$|\Psi_B >= e^{-\alpha \hat{T}} |\psi_{U=\infty} > \tag{4.2}$$

where α is the variational parameter and $\hat{T} = -t \sum_{<i,j>} \left(\hat{b}_i^\dagger \hat{b}_j + h.c. \right)$ with t as the hopping parameter between nearest neighbouring sites; $< i, j >$ on real space.

The operator $\hat{T}$ can be also represented on momentum space as; $\hat{T} = -t \sum_{k=0}^{L} 2 \cos\left(\frac{2\pi}{L} k\right)$ with L being the lattice size.

The term $e^{-\alpha \hat{T}}$ is called the Baeriswyl projection operator and we projected it on $U = \infty$ state, i.e. over a localized state [47].

4.2.2 Gutzwiller-Baeriswyl Projection

The Gutzwiller-Baeriswyl variational wavefunction is defined as;

$$|\Psi_{GB} >= e^{-\gamma \hat{N}} e^{-\alpha \hat{T}} |\psi_{U=\infty} > \tag{4.3}$$

where γ is the second variational parameter, and $\hat{N} = \sum_{i=0}^{L} n_i (n_i - 1)$ with $n_i = \hat{b}_i^\dagger \hat{b}_i$ on real space.

The term $e^{-\gamma \hat{N}}$ is called the Gutzwiller projection operator for a bosonic system [48].

This wavefunction is similar to the one which Otsuka suggested for fermionic systems [49];

$$|\Psi_{GB}>= e^{-\alpha \hat{T}} e^{-\gamma \hat{N}} |\phi> \tag{4.4}$$

where in this case ϕ is the non-interacting Fermi sea.

Note that $e^{-\gamma} = 0$ corresponds to the insulating state for fermions [50].

4.2.3 Calculation of The Observables

In order to calculate the observables, we introduce three different coordinates as left, i.e. x_L, center , i.e. x_C, right , i.e. x_R, for each single particle.

These coordinates form a complete set, i.e.

$$\sum_{i=0}^{L} |x_L >< x_L| = 1 \tag{4.5}$$

where L is the lattice site, and same condition also applies for center and right coordinates.

As expectation value, in the most general form, can be written as;

$$< \hat{A} >= \frac{< \Psi_{tr}|\hat{A}|\Psi_{tr} >}{< \Psi_{tr}|\Psi_{tr} >} \tag{4.6}$$

where Ψ_{tr} is variational wavefunction.

1. The expectation value for the Baeriswyl projection:

   The operator $\hat{A}$ is considered as diagonal in real space.

$$\begin{aligned} < \hat{A} > &= \frac{\sum_{L,C,R} < \Psi_\infty | x_L >< x_L | e^{-\alpha \hat{T}} | x_C >< x_C | \hat{A} | x_C >< x_c | e^{-\alpha \hat{T}} | x_R >< x_R | \Psi_\infty >}{\sum_{L,C,R} < \Psi_\infty | x_L >< x_L | e^{-\alpha \hat{T}} | x_C >< x_c | e^{-\alpha \hat{T}} | x_R >< x_R | \Psi_\infty >} \\ &= \frac{\sum_{L,C,R} P\left(x_L, x_C, x_R\right) \hat{A}\left(x_C\right)}{\sum_{L,C,R} P\left(x_L, x_C, x_R\right)} \end{aligned} \tag{4.7}$$

   where L, C, and R stands for left, center, and right coordinates.

   The probability function for an accepted move in (4.7) can be written as;

$$P\left(x_L, x_C, x_R\right) = \Psi_\infty\left(x_L\right) \Psi_\infty\left(x_R\right) K\left(|x_L - x_C|\right) K\left(|x_C - x_R|\right) \tag{4.8}$$

   where $\Psi_\infty\left(x_L\right) =< \Psi_\infty | x_L >$, and the propagator K is defined as;

$$K\left(|x - x^{'}|\right) =< x | e^{-\alpha \hat{T}} | x^{'} >= \prod_{i=1}^{L} < x_i | e^{-\alpha \hat{T}^{(1)}} | x_i^{'} > \tag{4.9}$$

   with $\hat{T}^{(1)}$ being the single particle operator.

   By using the fact that the operator $\hat{T}^{(1)}$ is diagonal in momentum space, one can write propagator in this space as;

$$K\left(|x - x^{'}|\right) = \prod_{i=1}^{L} \sum_{k=1}^{L} \frac{1}{L} e^{-\alpha \epsilon_k} e^{ik\left(x_i^{'} - x_i\right)} \tag{4.10}$$

   where $\epsilon_{k_n} = -2t \cos\left(\frac{2\pi n}{L} x\right)$ with n=0,..,L-1.

2. Expectation value for the Gutzwiller-Baeriswyl projection:

   The operator $\hat{A}$ is considered as diagonal in real space.

$$\begin{aligned} < \hat{A} > &= \frac{\sum_{L,C,R} \Psi_\infty(x_L) K\left(|x_L - x_C|\right) e^{-\gamma \hat{N}(x_C)} \hat{A}(x_C) e^{-\gamma N(\hat{x}_C)} K\left(|x_C - x_R|\right) \Psi_\infty(x_R)}{\sum_{L,C,R} \Psi_\infty(x_L) < x_L|e^{-\alpha \hat{T}}|x_C >< x_C|e^{-2\gamma \hat{N}}|x_C >< x_C|e^{-\alpha \hat{T}}|x_R > \Psi_\infty(x_R)} \\ &= \frac{\sum_{L,C,R} \widetilde{P}\left(x_L, x_C, x_R\right) \hat{A}\left(x_C\right)}{\sum_{L,C,R} \widetilde{P}\left(x_L, x_C, x_R\right)} \end{aligned} \tag{4.11}$$

   where $\widetilde{P}\left(x_L, x_C, x_R\right) = P\left(x_L, x_C, x_R\right) e^{-2\gamma N(\hat{x}_C)}$.

Note that dealing with expectation values introduces the products of exponential operators which is similar to the Suzuki-Trotter decomposition of $e^{-\tau \hat{H}}$, where $\hat{H} = \hat{T} + \hat{V}$ with kinetic and potential energies respectively, which is seen in QMC simulations [46].

As a cost of using variational theory, one needs to minimize the energy relation with respect to the variational parameter(s) so that we can obtain a configuration which is close to the exact ground state, i.e. $< \hat{H}_0 > \leq < \hat{H}_0 >_{tr}$, where $< \hat{H}_0 >$ stands for the exact ground state and $< \hat{H}_0 >_{tr}$ stands for the approximated ground state with a suitable variational wavefunction.

4.2.3.1 Calculation of Kinetic Energy, Potential Energy and Superfluid Density

In this section, calculations of energies and superfluid density are demonstrated only for the Baeriswyl projection. For the Gutzwiller-Baeriswyl projection, similar calculations can be done on potential energy and superfluid density. Kinetic energy relation with the Gutzwiller-Baeriswyl projection, on the other hand, is different with Gutzwiller factor which will be demonstrated later.

1. Potential Energy Calculation:

   On-site term of the Bose-Hubbard Hamiltonian is $\hat{V} = \frac{U}{2}\sum_{i=1}^{L}\hat{n_i}\left(\hat{n_i}-1\right)$. Note that potential energy is already diagonal in real space; hence,

$$\hat{V} = \frac{U}{2}\frac{\sum_{L,C,R} P\left(x_L, x_C, x_R\right)\hat{n}_i\left(x_C\right)\left[\hat{n}_i\left(x_C\right)-1\right]}{\sum_{L,C,R} P\left(x_L, x_C, x_R\right)} \tag{4.12}$$

2. Superfluid Density Calculation:

   Based on the last idea used in Section-2, we can calculate the superfluid fraction. We need to calculate the square root of the single particle spread function, which is also called *single particle delocalization* [51]. Spread function is

$$< \hat{\sigma}^2 >= \frac{-2}{\left(\Delta K\right)^2} Re\left\{ ln < e^{-i\Delta K\hat{X}} > \right\} \tag{4.13}$$

   where $\Delta K = \frac{2\pi}{L}$ is a shift in momentum, and $\hat{X}$ represents one-body position shift operator.

   Re-express the momentum shift operator for a more computationally oriented way with the Euler's formula gives

$$< e^{i\Delta K\hat{X}} >=< \cos\left(\Delta K\hat{X}\right) > + i < \sin\left(\Delta K\hat{X}\right) >=< Ce^{i\varphi} > \tag{4.14}$$

   where C is the magnitude and ϕ is the argument of the spread function. Hence,

$$< \hat{\sigma}^2 >= \frac{1}{\left(\Delta K\right)^2} ln\left[< \cos\left(\Delta K\hat{X}\right) >^2 + < \sin\left(\Delta K\hat{X}\right) >^2 \right] \tag{4.15}$$

   with $\hat{X} = \sum_{i=1}^{L} x_i\left(x_C\right)$.

Hence the single particle delocalization that contributes to the superfluid weight is

$$\frac{\sigma}{L} = \sqrt{< \hat{\sigma}^2 >} \tag{4.16}$$

3. Kinetic Energy Calculation For Baeriswyl Projection:

   We calculated the kinetic energy observable in two ways;

   (a) By taking derivative with respect to the variational parameter, α;

$$\begin{aligned} < \hat{T} > &= -\frac{\partial}{\partial\,(2\alpha)} ln < \Psi_\infty | e^{-2\alpha \hat{T}} | \Psi_\infty > \\ &= -\frac{1}{2} \frac{1}{\sum_{L,C,R} P\,(x_L, x_C, x_R)} \{ \sum_{L,C,R} P\,(x_L, x_C, x_R) \ldots \\ \ldots &\quad \left[\frac{1}{K\,(|x_L - x_C|)} \frac{\partial}{\partial \alpha} K\,(|x_L - x_C|) + \frac{1}{K\,(|x_C - x_R|)} \frac{\partial}{\partial \alpha} K\,(|x_C - x_R|) \right] \} \end{aligned} \tag{4.18}$$

   (b) By implementing the kinetic energy term directly;

   Define:

$$\sum_{<i,j>} \hat{b}_i^\dagger \hat{b}_i \equiv \sum_{C,C'} |x_C^{'} >< x_C| \tag{4.19}$$

   Then, substitute (4.18) with its hermitian conjugate to (4.7); hence,

$$< \hat{T} >= \frac{\sum_{L,C,C',R} P\,(x_L, x_C, x_R) \left[\frac{K\left(|x_L - x_{C'}|\right)}{K(|x_L - x_C|)} + \frac{K\left(|x_{C'} - x_R|\right)}{K(|x_C - x_R|)} \right]}{\sum_{L,C,R} P\,(x_L, x_C, x_R)} \tag{4.20}$$

4. Kinetic Energy Calculation For Gutzwiller-Baeriswyl Projection:

   For this case, we cannot use the first approach showed in (4.2.3.1.3.a); because for different site indices, i.e. $i \neq j$, the operators $\hat{T}$ and $\hat{N}$ do not commute, i.e. $\left[\hat{T}, \hat{N}\right] \neq 0$. Hence, we need to use the kinetic energy formulation explained in (4.2.3.1.3.b) by adding the Gutzwiller correction.

   Substitute (4.18) into (4.11), and note that the operator $\hat{N}$ is diagonal in real space;

$$< \hat{T} >= \frac{\sum_{L,C,C',R} \widetilde{P}\left(x_L, x_C, x_R\right) \left[\frac{K\left(|x_L - x_{C'}|\right)}{K(|x_L - x_C|)} + \frac{K\left(|x_{C'} - x_R|\right)}{K(|x_C - x_R|)}\right] \frac{e^{-\gamma \hat{N}\left(x_{C'}\right)}}{e^{-\gamma \hat{N}(x_C)}}}{\sum_{L,C,R} \widetilde{P}\left(x_L, x_C, x_R\right)} \tag{4.21}$$

Chapter 5

Data Analysis and Conclusion

In this chapter, results of the VMC techniques applied to the one dimensional Bose-Hubbard model with projected wavefunctions; namely, *Baeriswyl* and *Gutzwiller-Baeriswyl*, are analysed.

As a requirement of the VMC approach, we need to propose a trial wavefunction in order to analyse the ground state properties of the Bose-Hubbard model. Depending on the variational parameter attained to each trial wavefunction, one obtains a set of ground state energies. Among them, the lowest energy state must be chosen, which is described by the best trial wavefunction. In order to choose such a wavefunction, one needs to optimise the energy as a function of the parameter(s); which can be done via methods; *steepest descent*, *parallel tempering Monte Carlo*, *energy variance minimization*, or *conjugate gradient*.

In order to observe the ground state properties of the system with the projected wavefunctions, we, first, minimise the energy considering the different choices of the hopping parameter, $t>0$. Then, we introduce a hypothetical chemical potential, since we are working on the canonical ensemble, as [4];

$$\mu\left(N\right) = E\left(N+1\right) - E\left(N\right) \tag{5.1}$$

Hence, we can and will study the ground state phase diagram of the Bose-Hubbard model.

How we control the number of particles is implemented in the algorithm we developed, which is imposed on the ψ_∞, regardless of the hypothetical chemical potential that we introduced.

To study the ground state phase diagram of the model, we introduced two different variational wavefunctions. First, we analyse the system with the Baeriswyl projected wavefunction, then, we re-analyse the system with a Gutzwiller correction imposed on the Baeriswyl projected wavefunction.

5.1 Baeriswyl Projection Results

Baeriswyl wavefunction, stated in (4.2), is projected onto a localized state and is supposed to introduce hoppings between sites. These hoppings are controlled with the parameter t, as well as α and U. We analysed a system having lattice sites as $L = 20$ with particle number $N = [1, 60]$ and then $L = 40$ with particle number $N = [1, 160]$. Larger lattice site is considered only for the single particle delocalization function, i.e. (4.15).

In order to observe how single particle level is delocalizing with the Baeriswyl projection, one can check the propagator, i.e. (4.10), behavior as;

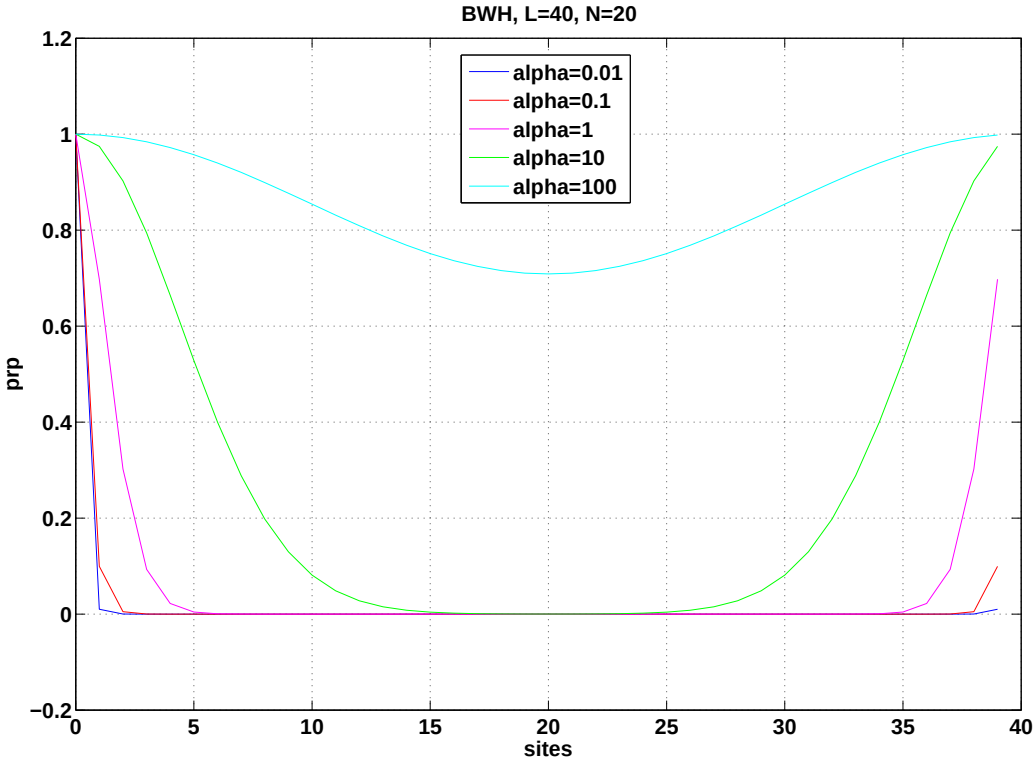

Figure 5.1: Propagator vs lattice site for Baeriswyl projection.

Observe that as α gets large, single particle propagator starts to delocalize.

Before presenting the phase diagram for the Baeriswyl projection, we checked indirectly that whether a quantum phase transition occurs before introducing the hypothetical chemical potential, i.e. μ in (5.1). Below, one can see how the total ground state energy of the Baeriswyl wavefunction changes with respect to α when we scan over different choices of the hopping parameter for a system with $L = 40$;

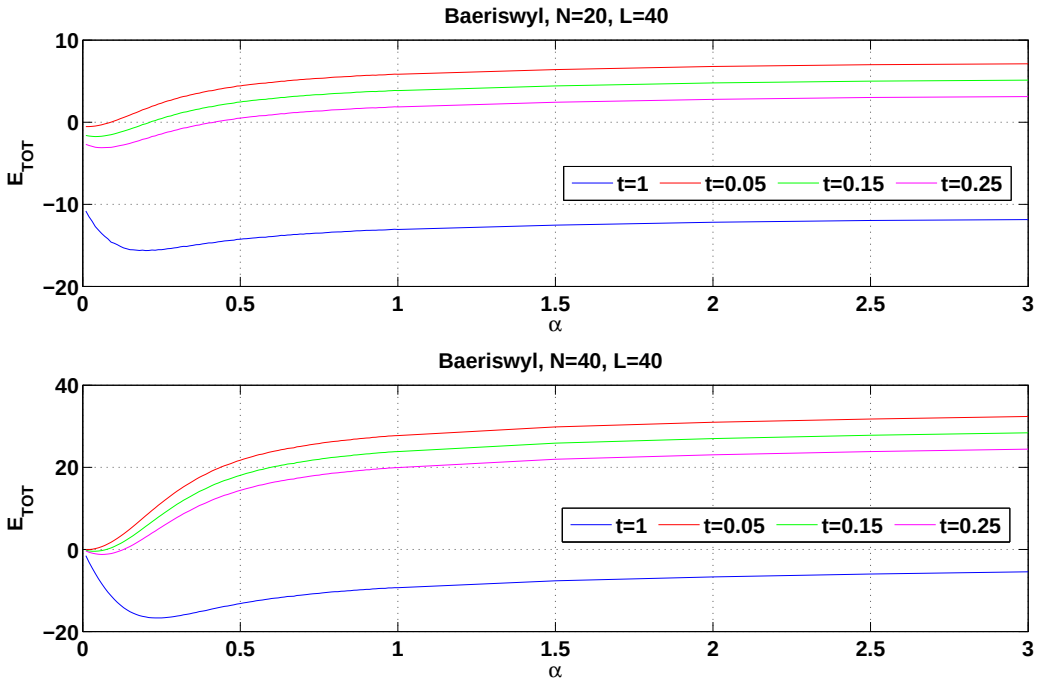

Figure 5.2: E_{TOT} vs α for Baeriswyl projection.

In Fig.5.2, even though α is just a variational parameter, it is an indication of the order parameter because each α value defines a specific wavefunction, i.e. (4.2) and (4.3), and thus, we would have an order parameter associated to that specific α value. Based on this logic, we do not see any phase transition neither first nor second order. We observe that a global minimum occurs and migrates for larger values of t.

The phase diagram for the Baeriswyl projection with $L = 40$ lattice sites can be seen in Fig.5.3.

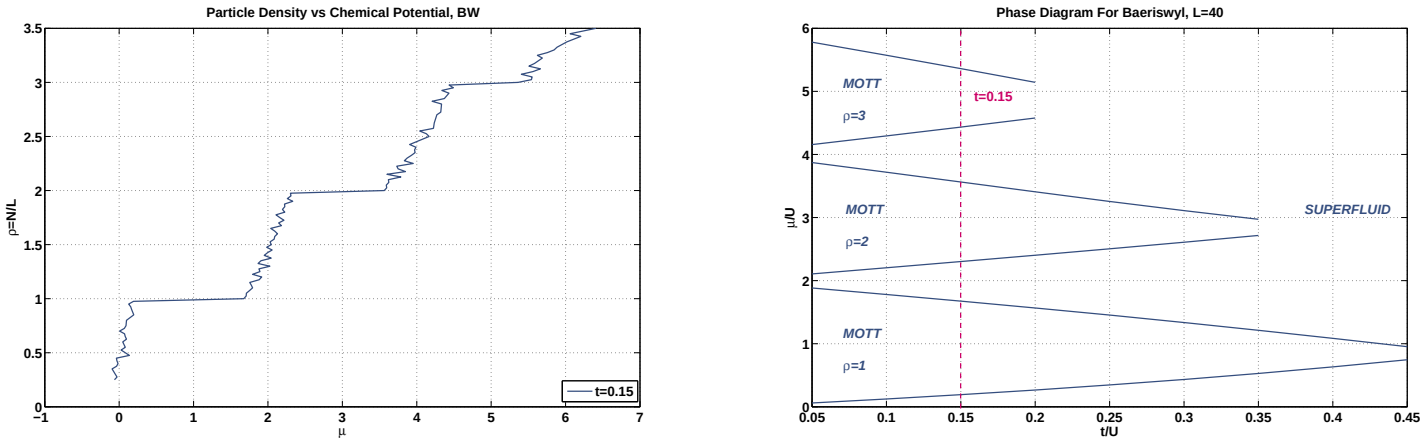

Figure 5.3: Phase diagram for Baeriswyl projection with $L = 40$.

In Fig.5.3, on the left hand side, we see that for a specific value of the hopping parameter which is chosen arbitrarily how the phase diagram on the right hand side occurs. Observe that for integer values of the boson density, we have a finite range in μ which does not affect the boson density. This case corresponds to the Mott insulating phase. Whereas, for non-integer values of the boson density, we do not have a constant ratio of ρ which corresponds to the superfluid phase.

To see how system size affects the phase diagram, observe Fig.5.4 for a system having $L = 20$ lattice sites;

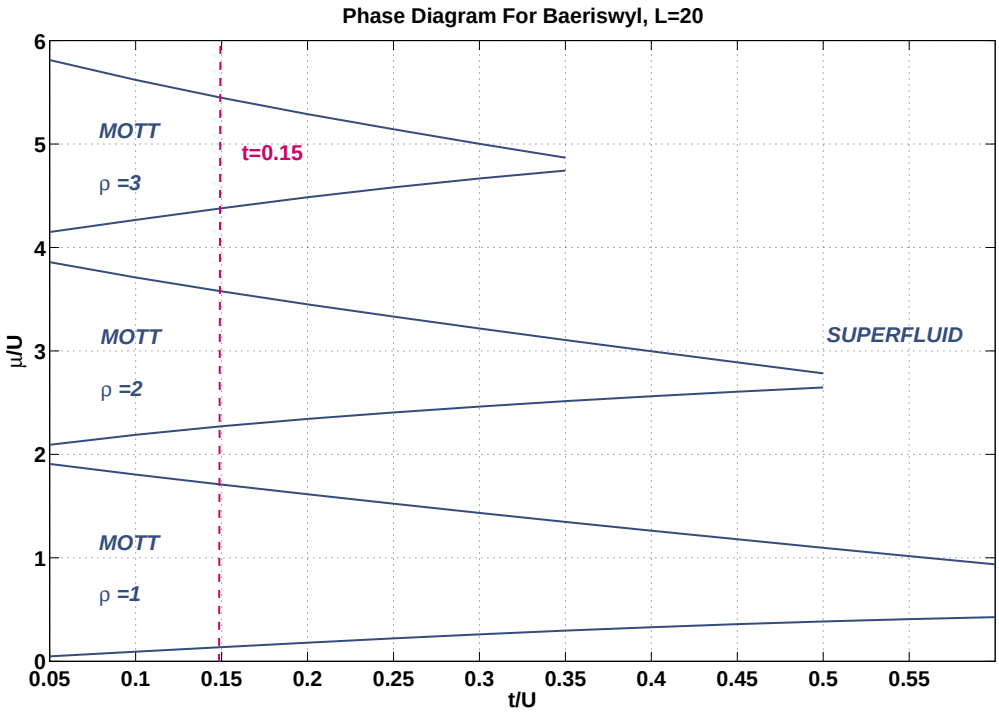

Figure 5.4: Phase diagram for Baeriswyl projection with $L = 20$.

See that the tip of the Mott insulating lobes are different depending on the system size, which gives better results [19] for the larger system size.

5.2 Gutzwiller-Baeriswyl Projection Results

Gutzwiller-Baeriswyl wavefunction, stated in (4.3), is projected onto a localized state and is supposed to introduce hoppings between sites as in the case of Baeriswyl projection. For the Gutzwiller-Baeriswyl projection, we analysed a system having lattice sites as $L = 40$ with particle number $N = [1, 160]$. Larger lattice site is considered only for the single particle delocalization function, i.e. (4.15).

Again, before presenting the phase diagram for the Gutzwiller-Baeriswyl projection, we checked indirectly that whether a quantum phase transition occurs before

introducing the hypothetical chemical potential, i.e. μ in (5.1). Below, one can see how the total ground state energy of the Gutzwiller-Baeriswyl wavefunction changes with respect to α when we scan over different choices of the hopping parameter for a system with $L = 40$;

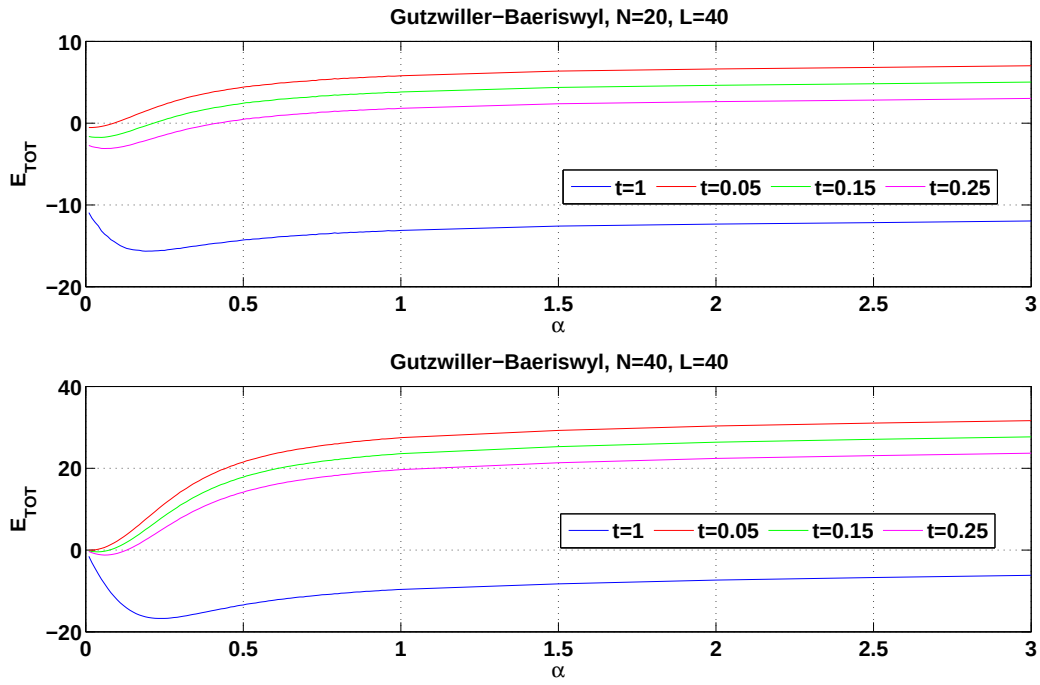

Figure 5.5: E_{TOT} vs α for Gutzwiller-Baeriswyl projection with $\gamma = 0.01$.

In Fig.5.5, we again observe that a global minimum occurs and migrates for larger values of α. Hence, we do not have any phase transition, neither first nor second order as in the Baeriswyl results.

The phase diagram for the Gutzwiller-Baeriswyl projection with $L = 40$ lattice sites can be seen in Fig.5.7.

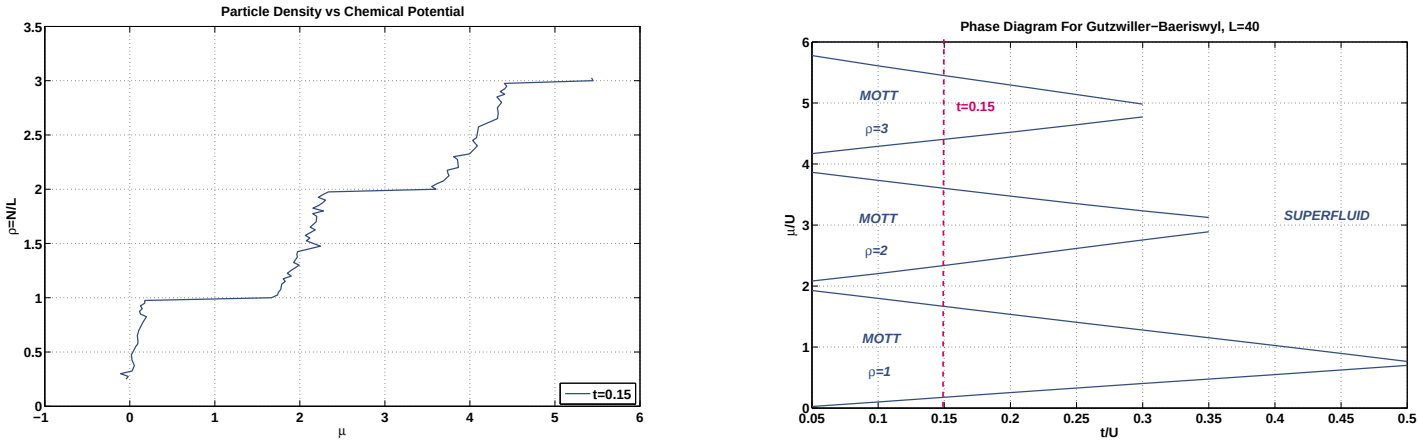

Figure 5.6: Phase diagram for Gutzwiller-Baeriswyl projection with $L = 40$.

In Fig.5.7, as in Fig.5.3, on the left hand side, we see that for a specific value of the hopping parameter which is chosen arbitrarily how the phase diagram on the right hand side occurs. Observe that for integer values of the boson density, we have a finite range in μ which again does not affect the boson density. This case corresponds to the Mott insulating phase. Whereas, for non-integer values of the boson density, we do not have a constant ratio of ρ which corresponds to the superfluid phase.

As a comparison between the two projectors that we applied to the Bose-Hubbard model with same lattice sites, i.e. $L = 40$, see Fig.5.8;

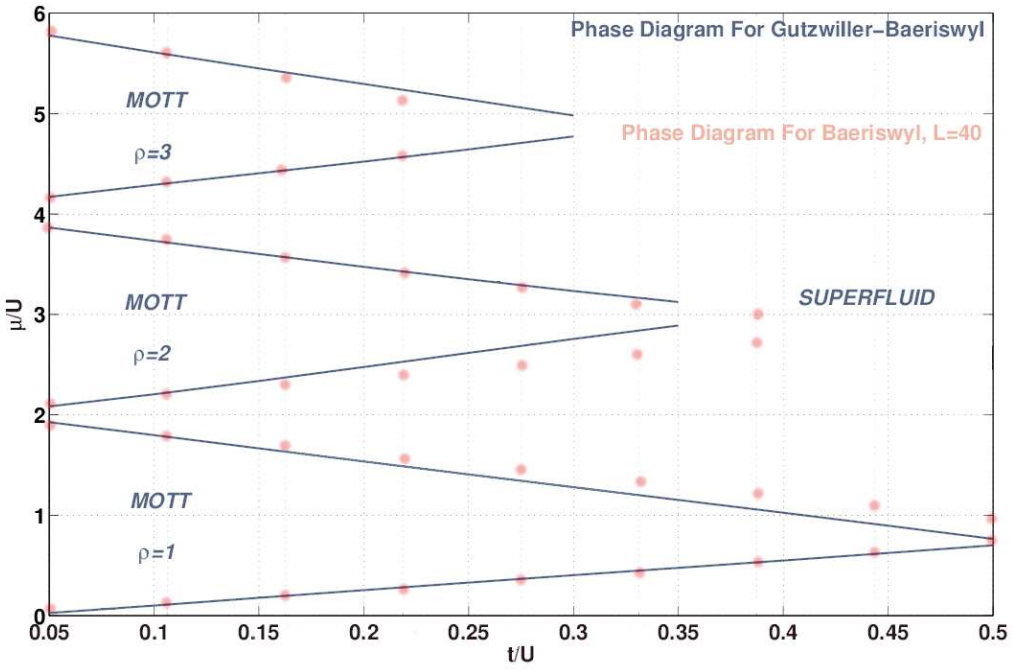

Figure 5.7: Phase diagram comparison between Gutzwiller and Gutzwiller-Baeriswyl projections with $L = 40$

The red one with dots belongs to the Baeriswyl results and the blue one with solid lines belongs to the Gutzwiller-Baeriswyl results.

In the PRB paper of Freericks and Monien in 1995, they found the critical value for the Mott lobe as $\frac{t}{U} = 0.215 \pm 0.01$ [19] by applying the QMC techniques. Even though our results are far beyond what they found, the tips for the Mott lobes are closer to their value for the Gutzwiller-Baeriswyl projection.

5.3 Conclusion

In this chapter, we analysed the results that we obtained from both the Baeriswyl and Gutzwiller-Baeriswyl projections for the one dimensional Bose-Hubbard model even though our method is applicable to any dimension.

Figures 5.2 and 5.5, on the other hand, indicate that for a fixed number of particles, both in commensurate and incommensurate fillings, we do not have phase transition. Hence, we need to introduce another on-site potential, i.e. μ, to control the particle fluctuation and encourage phase transition.

The phase diagrams obtained for both projections give qualitatively good results compared to the results of Freericks and Monien [19] and Scalettar et al. [4]; however, our results are quantitatively weak as the critical t value for the Baeriswyl result is ~ 0.45; whereas for the Gutzwiller-Baeriswyl it is ~ 0.5. Although we expect that the Gutzwiller correction to the Baeriswyl projection would improve the critical t value for the tip of the Mott lobes, it gave no good contribution. In order to fix this problem Monte Carlo steps might be increased or different optimization methods, other than minimization of the energy as indicated at the beginning of this chapter, can be done on the projected wavefunctions.

Regarding to the quantitative calculations, our results show that variational Monte Carlo approach with Baeriswyl and Gutzwiller-Baeriswyl projections do give rough results rather than exact. However, the chosen lattice size, which is at most $L = 40$ for general expectation values might affect the results. As we can observe from the phase diagrams of different lattice sizes, i.e. Fig.5.3 and Fig.5.4, critical value of t changes, and as the lattice size gets bigger, it gives more accurate results regarding to the result in [19].

Future work might include trying these projected wavefunctions with other Monte Carlo methods; like diffusion Monte Carlo or path integral Monte Carlo, which is more common, and see if it gives better results. Preferentially, if variational Monte Carlo is going to be used as a method, one can check how dimensionality, larger Monte Carlo steps, or larger system size affects the results compared to the ones we obtained in this thesis.

Bibliography

[1] D. Jaksch, C. Bruder, J. I. Cirac, C. W. Gardiner, and P. Zoller, "Cold bosonic atoms in optical lattices," *Phys. Rev. Lett.*, vol. 81, pp. 3108–3111, Oct 1998.

[2] A. van Oudenaarden and J. E. Mooij, "One-dimensional mott insulator formed by quantum vortices in josephson junction arrays," *Phys. Rev. Lett.*, vol. 76, pp. 4947–4950, Jun 1996.

[3] R. Baltin and K.-H. Wagenblast, "Quantum phase transitions for bosons in one dimension," *Europhys. Lett.*, vol. 39, no. 1, pp. 7–12, 1997.

[4] R. T. Scalettar, G. Batrouni, P. Denteneer, F. H©bert, A. Muramatsu, M. Rigol, V. Rousseau, and M. Troyer, "Equilibrium and dynamical properties of the boson hubbard model in one dimension," *Journal of Low Temperature Physics*, vol. 140, no. 3-4, pp. 313–332, 2005.

[5] E. L. Pollock and D. M. Ceperley, "Path-integral computation of superfluid densities," *Phys. Rev. B*, vol. 36, pp. 8343–8352, Dec 1987.

[6] J. Cao, "Winding-number effect in path-integral simulations," *Phys. Rev. E*, vol. 49, pp. 882–889, Jan 1994.

[7] W. Kohn, "Theory of the insulating state," *Phys. Rev.*, vol. 133, pp. A171–A181, Jan 1964.

[8] B. S. Shastry and B. Sutherland, "Twisted boundary conditions and effective mass in heisenberg-ising and hubbard rings," *Phys. Rev. Lett.*, vol. 65, pp. 243–246, Jul 1990.

[9] B. Hetenyi, "Drude weight, meissner weight, rotational inertia of bosonic superfluids: How are they distinguished?," *Journal of the Physical Society of Japan*, vol. 83, no. 3, p. 034711, 2014.

[10] B. Hetényi, "dc conductivity as a geometric phase," *Phys. Rev. B*, vol. 87, p. 235123, Jun 2013.

[11] J. Hubbard, "Electron correlations in narrow energy bands," *Proceedings of the Royal Society of London. Series A, Mathematical and Physical Sciences*, vol. 276, no. 1365, pp. pp. 238–257, 1963.

[12] H. A. Gersch and G. C. Knollman, "Quantum cell model for bosons," *Phys. Rev.*, vol. 129, pp. 959–967, Jan 1963.

[13] M. P. A. Fisher, P. B. Weichman, G. Grinstein, and D. S. Fisher, "Boson localization and the superfluid-insulator transition," *Phys. Rev. B*, vol. 40, pp. 546–570, Jul 1989.

[14] p. a. y. Wen Xiao Gang, title=Quantum Field Theory of Many-Body Systems: From the Origin of Sound to an Origin of Light and Electrons.

[15] S. Sachdev, *Quantum phase transitions*. Cambridge: Cambridge University Press, second ed. ed., 2011.

[16] J. M. Zhang and R. X. Dong, "Exact diagonalization: the bose–hubbard model as an example," *Europhys. Lett.*, vol. 31, no. 3, pp. 591–602, 2010.

[17] T. Comparin, *Numerical study of the trapped and extended Bose-Hubbard models*. PhD thesis, Utrecht University, 2013.

[18] I. Bloch, J. Dalibard, and W. Zwerger, "Many-body physics with ultracold gases," *Rev. Mod. Phys.*, vol. 80, pp. 885–964, Jul 2008.

[19] J. K. Freericks and H. Monien, "Strong-coupling expansions for the pure and disordered bose-hubbard model," *Phys. Rev. B*, vol. 53, pp. 2691–2700, Feb 1996.

[20] A. J. Leggett, "Bose-einstein condensation in the alkali gases: Some fundamental concepts," *Rev. Mod. Phys.*, vol. 73, pp. 307–356, Apr 2001.

[21] P. Kapitza, "Viscosity of liquid helium below the -point," *Nature*, vol. 141, Jan 1938.

[22] R. Resta, "Quantum-mechanical position operator in extended systems," *Phys. Rev. Lett.*, vol. 80, pp. 1800–1803, Mar 1998.

[23] R. Resta and S. Sorella, "Electron localization in the insulating state," *Phys. Rev. Lett.*, vol. 82, pp. 370–373, Jan 1999.

[24] D. J. Scalapino, S. R. White, and S. Zhang, "Insulator, metal, or superconductor: The criteria," *Phys. Rev. B*, vol. 47, pp. 7995–8007, Apr 1993.

[25] H. M. J. K. Freericks, "Phase diagram of the bose hubbard model," *Europhys. Lett.*, vol. 26, no. 7, p. 545, 1994.

[26] H. Weimer, "Chapter 1: Exact diagonalization." This is an electronic document. http://www.itp.uni-hannover.de/ weimer/teaching/QSim2013/exact-diagonalization.pdf. Date retrieved: May 19, 2014.

[27] K. S. Pati, "Density matrix renormalization group method." This is an electronic document. http://www.jncasr.ac.in/ccms/nqm2007/lecturenotes/6day3nov/dmrg_Swapan.ppt. Date retrieved: May 19, 2014. Date last modified: May 20, 2014.

[28] E. Dagotto, "Correlated electrons in high-temperature superconductors," *Rev. Mod. Phys.*, vol. 66, pp. 763–840, Jul 1994.

[29] M. Suzuki, "Generalized trotter's formula and systematic approximants of exponential operators and inner derivations with applications to many-body problems," *Communications in Mathematical Physics*, vol. 51, no. 2, pp. 183–190, 1976.

[30] H. F. Trotter, "On the product of semi-groups of operators," *Proc. Am. Math. Soc*, vol. 10, no. 4, pp. 545–551, 1959.

[31] J. E. Hirsch, R. L. Sugar, D. J. Scalapino, and R. Blankenbecler, "Monte carlo simulations of one-dimensional fermion systems," *Phys. Rev. B*, vol. 26, pp. 5033–5055, Nov 1982.

[32] N. Prokof'ev, B. Svistunov, and I. Tupitsyn, "Exact quantum monte carlo process for the statistics of discrete systems," *Journal of Experimental and Theoretical Physics Letters*, vol. 64, no. 12, pp. 911–916, 1996.

[33] N. ProkofÄôev, B. Svistunov, and I. Tupitsyn, "Exact, complete, and universal continuous-time worldline monte carlo approach to the statistics of discrete quantum systems," *Journal of Experimental and Theoretical Physics*, vol. 87, no. 2, pp. 310–321, 1998.

[34] H. G. Evertz, G. Lana, and M. Marcu, "Cluster algorithm for vertex models," *Phys. Rev. Lett.*, vol. 70, pp. 875–879, Feb 1993.

[35] B. B. Beard and U.-J. Wiese, "Simulations of discrete quantum systems in continuous euclidean time," *Phys. Rev. Lett.*, vol. 77, pp. 5130–5133, Dec 1996.

[36] A. W. Sandvik and J. Kurkijärvi, "Quantum monte carlo simulation method for spin systems," *Phys. Rev. B*, vol. 43, pp. 5950–5961, Mar 1991.

[37] A. W. Sandvik, "Stochastic series expansion method with operator-loop update," *Phys. Rev. B*, vol. 59, pp. R14157–R14160, Jun 1999.

[38] S. R. White, "Density matrix formulation for quantum renormalization groups," *Phys. Rev. Lett.*, vol. 69, pp. 2863–2866, Nov 1992.

[39] S. R. White, "Density-matrix algorithms for quantum renormalization groups," *Phys. Rev. B*, vol. 48, pp. 10345–10356, Oct 1993.

[40] S. D. Drell, M. Weinstein, and S. Yankielowicz, "Quantum field theories on a lattice: Variational methods for arbitrary coupling strengths and the ising model in a transverse magnetic field," *Phys. Rev. D*, vol. 16, pp. 1769–1781, Sep 1977.

[41] U. Schollwöck, "The density-matrix renormalization group," *Rev. Mod. Phys.*, vol. 77, pp. 259–315, Apr 2005.

[42] N. Metropolis, A. W. Rosenbluth, M. N. Rosenbluth, A. H. Teller, and E. Teller, "Equation of state calculations by fast computing machines," *The Journal of Chemical Physics*, vol. 21, no. 6, 1953.

[43] W. L. McMillan, "Ground state of liquid he4," *Phys. Rev.*, vol. 138, pp. A442–A451, Apr 1965.

[44] M. C. Gutzwiller, "Effect of correlation on the ferromagnetism of transition metals," *Phys. Rev. Lett.*, vol. 10, pp. 159–162, Mar 1963.

[45] D. Ceperley, G. V. Chester, and M. H. Kalos, "Monte carlo simulation of a many-fermion study," *Phys. Rev. B*, vol. 16, pp. 3081–3099, Oct 1977.

[46] M. Suzuki, (Masuo), and 1937, *Quantum Monte Carlo methods in condensed matter physics /.* Singapore ;: World Scientific,, c1993.[reprited 1998].

[47] V. G. Rousseau, D. P. Arovas, M. Rigol, F. Hébert, G. G. Batrouni, and R. T. Scalettar, "Exact study of the one-dimensional boson hubbard model with a superlattice potential," *Phys. Rev. B*, vol. 73, p. 174516, May 2006.

[48] D. S. Rokhsar and B. G. Kotliar, "Gutzwiller projection for bosons," *Phys. Rev. B*, vol. 44, pp. 10328–10332, Nov 1991.

[49] H. Otsuka, "Variational monte carlo studies of the hubbard model in one- and two-dimensions –off-diagonal intersite correlation effects–," *Journal of the Physical Society of Japan*, vol. 61, no. 5, pp. 1645–1656, 1992.

[50] D. Baeriswyl, *Microscopic Aspects of Nonlinearity in Condensed Matter.* Springer, 1987.

[51] B. Hetényi, "Drude weight, meissner weight, rotational inertia of bosonic superfluids: How are they distinguished?," *Journal of the Physical Society of Japan*, vol. 83, no. 3, p. 034711, 2014.